Lattice Vibrations in Molybdenum

C. B. WALKER
Army Materials and Mechanics Research Center, Watertown, Massachusetts

AND

P. A. EGELSTAFF
Solid State Physics Division, U.K.A.E.R.E., Harwell, Berks., England

(Received 2 August 1968)

A neutron inelastic scattering study has been made of the normal modes of vibration of molybdenum in a $(1\bar{1}0)$ plane at room temperature using a cold-neutron chopper time-of-flight technique. The measured frequency–wave-vector results are in general agreement with the symmetry-axis data of Woods and Chen but show further anomalous behavior in several regions in this plane. The "normal" phonons (those not in anomalous regions) are fitted acceptably by Born–von Karman general force models that include at least six neighbors with a relatively large value for the sixth-neighbor force constant. The anomalous regions appear to be examples of Kohn anomalies, and two of these are interpreted on this basis to give information on dimensions of the near-planar sections of the Lomer model of the Fermi surface.

INTRODUCTION

A NEUTRON inelastic scattering study has been made of the frequency–wave-vector dispersion relations of phonons in the $(1\bar{1}0)$ plane in molybdenum at room temperature using a cold-neutron chopper time-of-flight technique. Molybdenum was chosen as the material to be studied because of its high symmetry (monatomic bcc), its relatively favorable nuclear properties, its availability in single-crystal form, and its then unknown lattice dynamics. During the course of the investigation, Woods and Chen[1] (WC) reported the results of a neutron triple-axis study of phonon dispersion along the major symmetry axes in molybdenum, and these results subsequently were augmented and further discussed by Woods[2] and Woods and Powell.[3] The most notable feature of the phonon dispersion was the anomalous behavior found in several regions, which was interpreted in terms of Kohn anomalies. The present measurements are in reasonably good agreement with these data, but they contain new information obtained from the off-symmetry-axis coverage, particularly regarding the anomalous regions, and our analysis has proceeded somewhat differently, so the results are presented here in some detail.

EXPERIMENTAL DETAILS

The experimental measurements were made on the "cold neutron apparatus" at the Harwell DIDO reactor using a vertical array of 24 ZnS-LiF scintillation detectors ranging from 35° to 91° in scattering angle. Details of the apparatus and the general procedures are given in several recent papers.[4–8] The molybdenum sample was a composite of three sections (each approximately 0.4 in. in diameter and 2.2 in. long) of a rather imperfect single crystal grown by electron beam melting with the $[1\bar{1}0]$ axis along the cylinder axis.[9] The crystallite distribution in the composite sample was such that $\frac{2}{3}$ of the diffracting power of a reflection was contained within $\pm\frac{3}{4}°$, with the extremes of the distribution extending approximately $\pm 2\frac{1}{2}°$.

All measurements were made with the $[1\bar{1}0]$ axis of the sample perpendicular to the vertical scattering plane, the orientation of the sample about this axis being changed in steps for the different runs. All the phonons observed thus had wave vectors lying in the $(1\bar{1}0)$ plane and belonged to one or the other of the two branches whose polarization vectors are contained in this plane. These two branches, labelled "high" and "low," are defined by the relative magnitudes of the phonon frequencies; the polarization in a branch may change discontinuously at points of degeneracy, but the frequency is a continuous function of the wave vector. Figure 1 illustrates the results obtained in an experimental run. The time-of-flight spectrum measured by one counter is given in Fig. 1(a), in this case showing three phonons. The data from all 24 counters for this run are plotted in reciprocal space in Fig. 1(b), where the particular scattering direction $\mathbf{k}$ drawn is that for which the data of Fig. 1(a) were obtained. The solid and open circles denote high- and low-branch phonons, respectively, and connecting lines are sketched in to clarify the shape of the scattering surfaces. Twenty such runs were made with sample orientations varied through

[1] A. D. B. Woods and S. H. Chen, Solid State Commun. **2**, 233 (1964).
[2] A. D. B. Woods, *Brookhaven National Laboratory Report No. 940* (U. S. Government Printing Office, Washington, D. C., 1966), p. 8.
[3] A. D. B. Woods and B. M. Powell, Phys. Rev. Letters **15**, 778 (1965).
[4] D. Harris, S. J. Cocking, P. A. Egelstaff, and F. J. Webb, in *Proceedings of the Chalk River Symposium on Inelastic Scattering of Neutrons in Solids and Liquids* (International Atomic Energy Agency, Vienna, 1963), Vol. 1, p. 107.
[5] G. Peckham, J. Phys. Chem. Solids Suppl. **1**, 49 (1965); Proc. Phys. Soc. (London) **90**, 657 (1967).
[6] S. K. Sinha, Phys. Rev. **143**, 422 (1966).
[7] D. Long Price, in *Proceedings of the Bombay Symposium on Inelastic Scattering of Neutrons* (International Atomic Energy Agency, Vienna, 1965), Vol. 1, p. 109.
[8] G. L. Squires, *Brookhaven National Laboratory Report No. 940* (U. S. Government Printing Office, Washington, D. C., 1966), p. 78.
[9] Purchased from Metals Research Ltd., Cambridge.

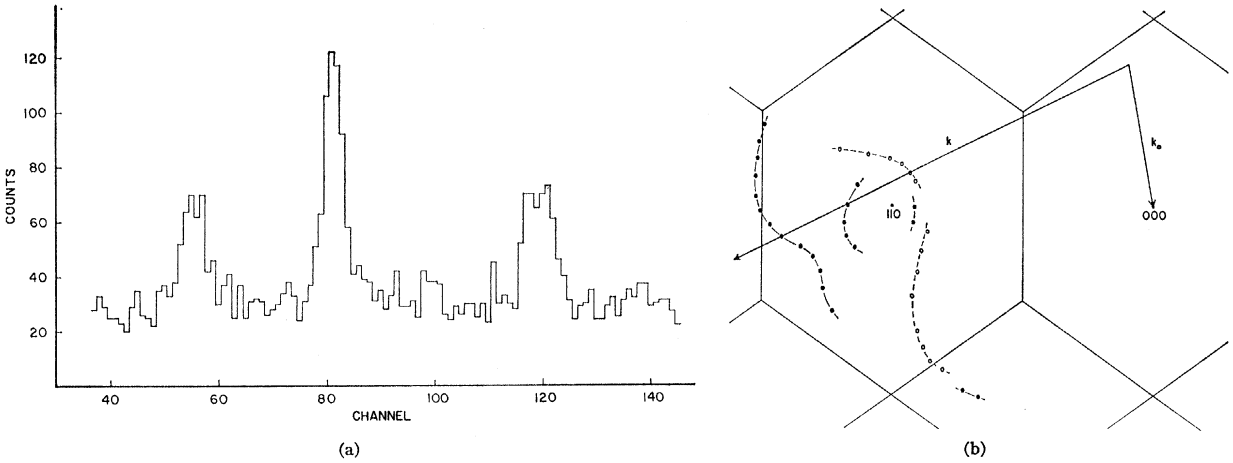

FIG. 1. (a) The time-of-flight spectrum for counter 8 in run 1945. The quantity plotted is the number of counts per 24 h in a sequence of 8-μsec-wide channels. (b) A plot in reciprocal space of all the phonons observed by the 24 counters in run 1945. The direction of scattering for counter 8 is shown by the vector **k**. The solid and open circles locate high- and low-branch phonons, respectively. The connecting lines sketch the shape of the scattering surfaces.

145°. The resulting time-of-flight spectra were analyzed with a least-squares Gaussian fitting program[10] to determine the peak positions, and the very broad, asymmetric or irregular phonon groups were discarded. Scattering-surface plots [e.g., Fig. 1(b)] were used to identify phonon branches and double scattering and overlapping phonon groups. Peak positions were corrected for sample shape and absorption and, where scattering surface curvature was large, corrections were also applied for sample mosaic spread, instrumental resolution, and variations in detector sensitivity and in the one-phonon scattering cross section, using preliminary values for a seven-neighbor general force model in the numerical scattering-surface calculations (see Appendix). Finally, the errors (both in frequency and in wave vector) from the various independent sources were combined to give an effective error in frequency alone using the relations

$$\Delta\nu_i = d\nu_i - \nabla\nu \cdot \mathbf{dq}_i$$

and

$$\Delta\nu = [\sum_i (\Delta\nu_i)^2]^{1/2},$$

where $\mathbf{dq}_i$ and $d\nu_i$ are the errors in wave vector and in frequency of a phonon due to the ith source.

Frequency–wave-vector values have been obtained in this way for 354 phonons, 179 in the high branch and 175 in the low branch, distributed irregularly through the rectangular area of the $(1\bar{1}0)$ plane irreducible under planar symmetry operations. The average effective standard deviation of the frequency of these phonons is 1.6%.

These data are in reasonably good agreement with the symmetry-axis measurements of WC, discrepancies for the most part being within $\pm 2\%$. Larger differences occur for some of the long-wavelength phonons ($\lambda^{-1} < 0.3a_0^{-1}$), particularly in the low branch, where the present frequencies tend to be generally higher by the order of 5%, but since both experimental approaches are subject to larger errors and corrections for instrumental resolution in this region, these differences are not considered to be important.

GROUPING AND ANALYSIS OF NORMAL PHONONS

Range of Forces

A least-squares fit was made to all the data for Born–von Karman general force models[11] of n neighbors where n was varied sequentially from 2–9. The quality of the fit for each model was determined first by examining a plot of the difference between experimental frequencies and frequencies calculated from the fitted model as a function of wave vector. Secondly, we used a statistical measure defined as

$$\text{FIT} = \sum[\Delta/\sigma]^2/[N_p - N_c - 1],$$

where Δ is the difference between the squares of the experimental and calculated frequencies, σ is the standard deviation of the square of the experimental frequency, and N_p and N_c are the number of phonons and the number of force constants in the model, respectively. For the statistical test, a good fit is said to be obtained when the sum of the squares of the weighted deviations is approximately equal to the number of degrees of freedom, i.e., when FIT$\simeq$1.

The results showed that no model gave a good fit to all the data. Models involving only the first few neighbors showed misfit over extensive regions of the plane. The smallest model to give a reasonable fit over most of

[10] The program, FIT AND SEARCH, written by G. Peckham, Ref. 5.

[11] M. Born and K. Huang, *Dynamical Theory of Crystal Lattices* (Oxford University Press, Oxford, 1954).

the area involved six neighbors, with a rather large sixth-neighbor force constant, and this model still gave significant misfit in a number of fairly small regions. The fit improved somewhat as seventh, eighth, and ninth neighbors were included, but each model still showed significant misfit, and this occurred in more or less the same regions where misfit to the six-neighbor model was found. Consequently, the (effective) restoring forces in molybdenum must include appreciable long-range components, their range being too great to allow analysis from these data.[12,13]

Fit to Normal Phonons

As an alternative procedure, we sought next to determine a model that would give a good fit to the data over the area of the plane outside of these persistent regions of misfit, both to obtain an approximate description of the shorter-range forces in this element and to establish a norm from which the misfit in the remaining regions could be measured. Then these remaining regions of misfit, called "anomalous" regions, would be considered separately by an entirely different approach.

TABLE I. Force-constant values (in 10^3 dyn/cm) for the seven-neighbor general force model for the normal phonon dispersion in molybdenum. The notation is that of Squires.[a]

Neighbor	Coordinates	Force constants	Radial component
1	(1,1,1)	$\alpha_1 = 15.82 \pm 0.12$ $\beta_1 = 12.00 \pm 0.41$	39.82
2	(2,0,0)	$\alpha_1 = 42.22 \pm 0.83$ $\alpha_2 = -1.54 \pm 0.34$	42.22
3	(2,2,0)	$\alpha_1 = 2.44 \pm 0.22$ $\alpha_3 = -0.57 \pm 0.30$ $\beta_3 = 1.92 \pm 0.54$	4.36
4	(3,1,1)	$\alpha_1 = -1.55 \pm 0.26$ $\alpha_2 = 0.14 \pm 0.09$ $\beta_1 = 0.76 \pm 0.10$ $\beta_2 = 0.58 \pm 0.21$	−0.47
5	(2,2,2)	$\alpha_1 = 0.74 \pm 0.11$ $\beta_1 = 0.36 \pm 0.22$	1.46
6	(4,0,0)	$\alpha_1 = 4.54 \pm 0.66$ $\alpha_2 = -0.51 \pm 0.28$	4.54
7	(3,3,1)	$\alpha_1 = 0.59 \pm 0.21$ $\alpha_3 = -0.84 \pm 0.29$ $\beta_1 = 0.11 \pm 0.07$ $\beta_3 = -0.45 \pm 0.41$	0.16

[a] Reference 13.

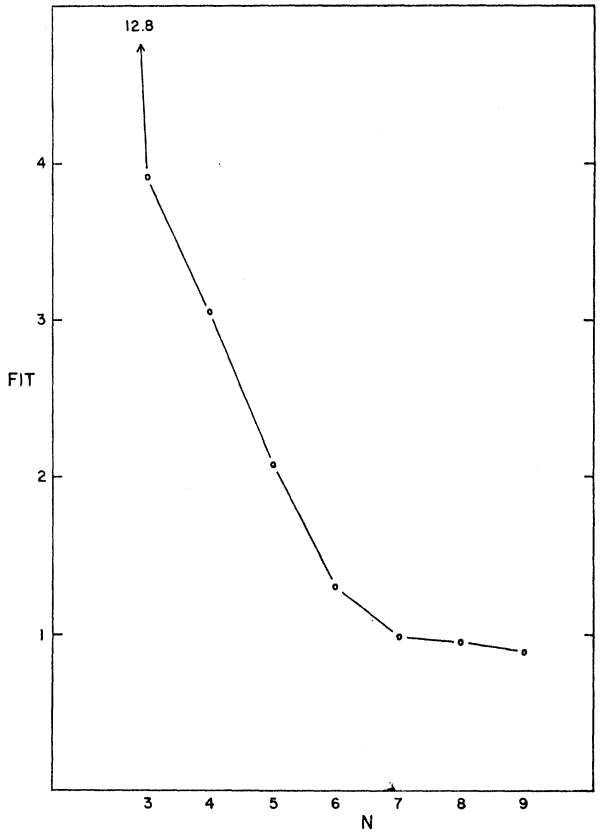

FIG. 2. Values of the parameter FIT for fits to the normal phonons as a function of the number of neighbors N in the general Born–von Karman model.

The regions of misfit found for $n \geq 6$ contained approximately one-fourth of all the observed phonons, a fraction large enough to have had an appreciable effect on the fits, even though the actual frequency misfits in most cases were no more than a few percent. Thus, the same least-squares analysis in terms of Born–von Karman general force models was repeated for just the "normal" phonons, excluding the phonons in the regions of misfit from the analysis. As before, the first model to give an acceptable fit was $n=6$, with a relatively large sixth-neighbor force constant. Inclusion of seventh neighbors improved the fit a little, while the addition of eighth and ninth neighbors made no significant difference, as could be expected. We chose the $n=7$ model to represent the normal phonon dispersion. Then, defining the "anomalous" regions as regions bounded by smooth curves within which the experimental and calculated frequencies for this model differed generally by two or more standard deviations, several further least-squares analyses were made in which a number of phonons on the edges of the anomalous regions were (a) included or (b) excluded from the fit. If the frequencies of such phonons calculated using the (b) force constants agreed within the errors with the experimental values, the phonons were called "normal"; otherwise they were left in the "anomalous" category. The final boundaries of the anomalous regions obtained in this way excluded 40 phonons in the high branch and 52 phonons in the low branch, leaving 139 normal phonons in the high branch and 123 in the low branch. The values of the parameter FIT obtained in fitting these normal phonons is plotted in Fig. 2 as a function of the number of neighbors in the model. The fit is satisfactory only for $n \geq 6$.

[12] Data in this plane can yield solutions only for models with no more than ten neighbors (Ref. 13).

[13] G. L. Squires, Arkiv Fysik **25**, 21 (1963).

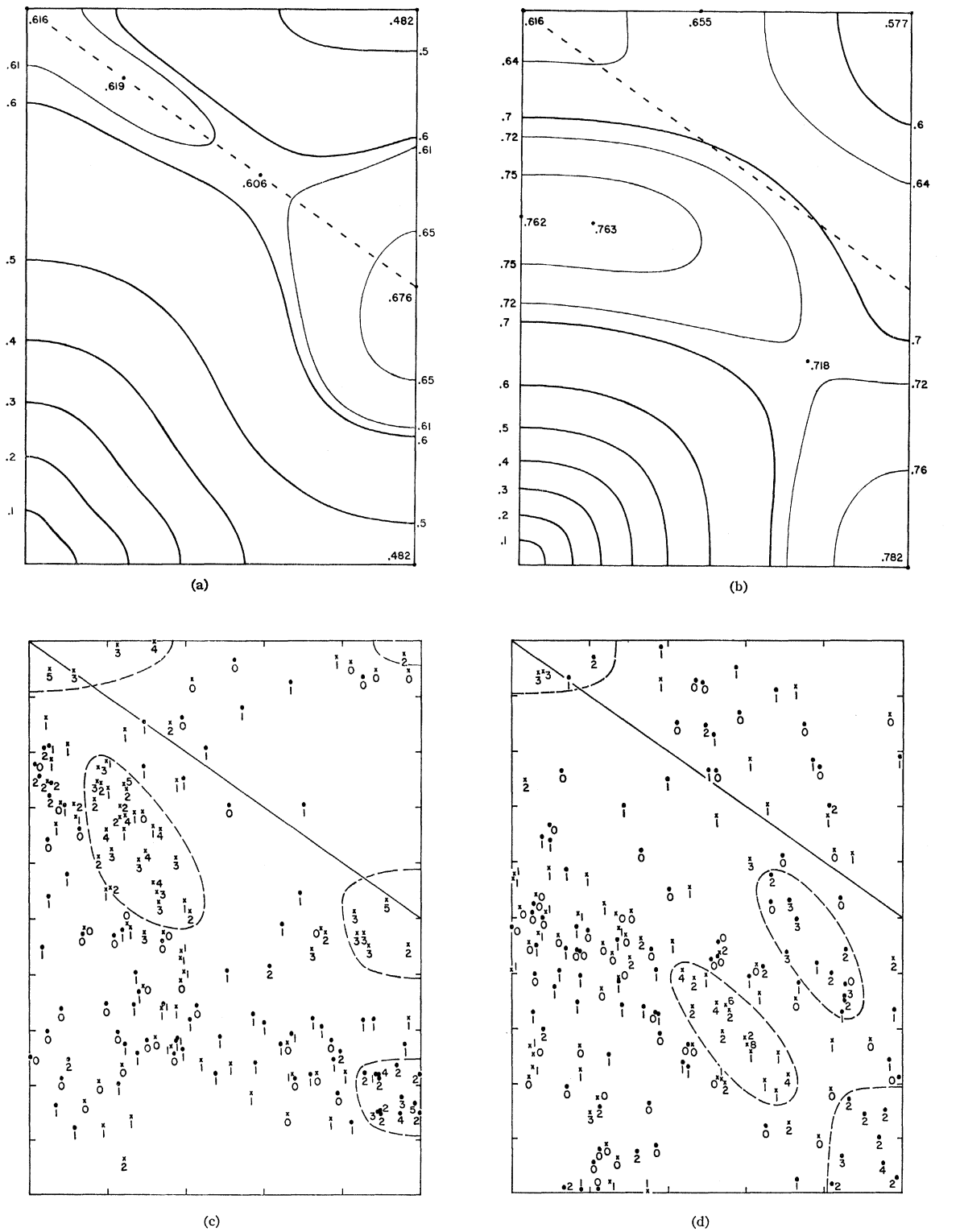

FIG. 3. (a) Constant-frequency contours for the low branch in the $(1\bar{1}0)$ plane calculated from the seven-neighbor model for the normal phonons. Frequencies are in units of 10^{13} cps. The wave-vector coordinate system is the usual one for this plane, as described in the text. (b) As in (a), but for the high branch. (c) Plots of the difference between experimental and calculated frequencies for each low-branch phonon, in units of its experimental standard deviation, at the position of its wave vector. The dashed lines mark the boundaries of the anomalous regions. (d) As in (c), but for the high branch. (e) As in (c), but the frequency differences are given as a percent of the calculated frequency. The dashed lines are contours of constant percentage misfit. (f) As in (e), but for the high branch.

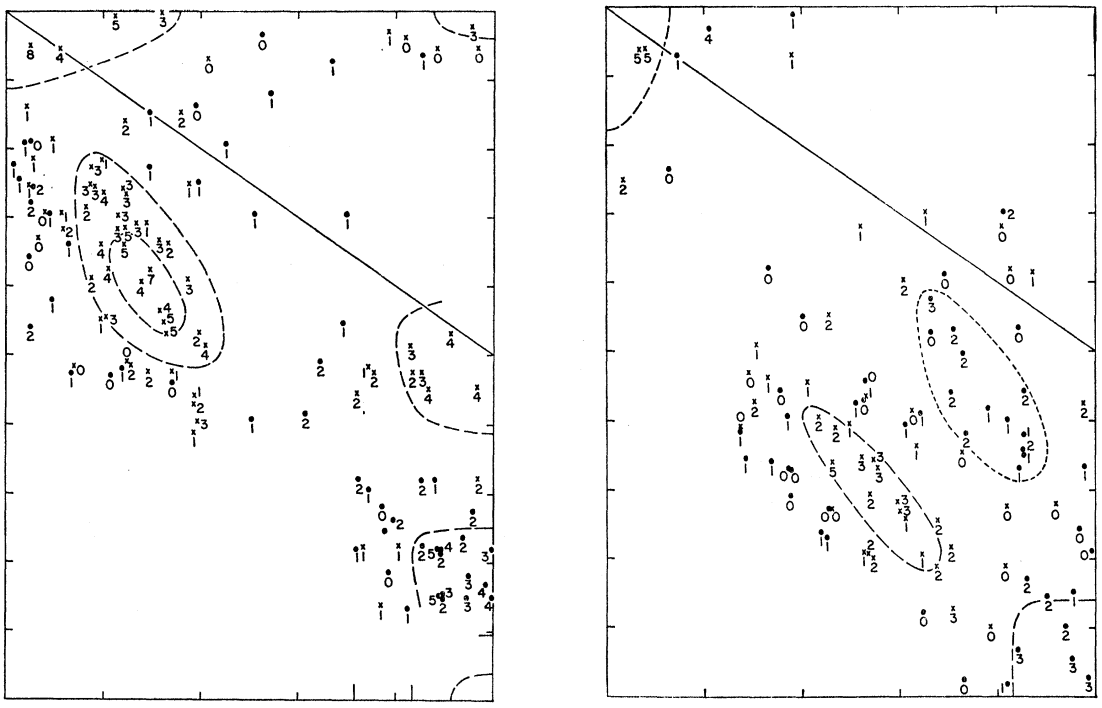

(e) (f)

FIG. 3. (*Continued.*)

Details of Seven-Neighbor Model

The seven-neighbor model fitted to these normal phonons yields the calculated normal dispersion for low- and high-branch phonons in the $(1\bar{1}0)$ plane shown by the respective plots of constant frequency contours in Figs. 3(a) and 3(b). The vertical and horizontal axes through the origin are the [001] and [110] axes, respectively, extending to the usual limits (Ref. 14), (0,0,1) and $(\frac{1}{2},\frac{1}{2},0)$; the dashed line shows that part of a [111] axis extending between $(\frac{1}{2},\frac{1}{2},\frac{1}{2})$ and (0,0,1). The two branches are degenerate by symmetry at (0,0,1) and $(\frac{1}{2},\frac{1}{2},\frac{1}{2})$ and by accident[15] on the boundary at approximately $(\frac{1}{2},\frac{1}{2},\frac{3}{4})$, so the polarization vectors show strong variations in the plane in the triangular area at the upper right. The results along the symmetry axes differ in some details from the calculated curves of WC, primarily because of the inclusion of more distant neighbors.

The fit of the individual phonons to this model is shown for the low and high branches in Figs. 3(c) and 3(d), respectively, where the difference between experimental and calculated frequencies for each phonon, in units of its experimental standard deviation, is plotted at the position of its wave vector. A solid circle denotes the coordinates of a phonon whose measured frequency is greater than that calculated from the model, while an X denotes a phonon whose measured frequency is less than that calculated. The number adjacent to a symbol gives the magnitude of the frequency difference, in units of the standard deviation, to the nearest integer. The dashed curves mark the boundaries of the anomalous regions; in several of these the consistency and magnitude of the misfit is quite striking. The mixed distribution of plus and minus differences for the normal phonons shows that the fit to these phonons is satisfactory; the size of these differences, which led to the result, FIT = 0.99, supports the evaluation of the experimental standard deviations as realistic.

The values of the force constants for this model are listed in Table I. The error given for each is the larger of (a) its standard deviation computed from the fit, or (b) one-half the largest departure from this force-constant value among the results obtained in fits with different "large" models (seven, eight, and nine neighbors), with various boundaries for the anomalous regions, or with the added restraint that the force constants yield the elastic constants of Bolef and de Klerk.[16] A radial component derived from these force constants is also tabulated for each neighbor to show the relative sizes of the forces. Three points about these force-constant values should be noted:

(1) The force-constant values given here do not differ appreciably from the force-constant values ob-

[14] In units of the cubic reciprocal cell edge.

[15] Due primarily to the large second-neighbor force constant.

[16] D. I. Bolef and J. de Klerk, J. Appl. Phys. **33**, 2311 (1962). Values differing from these by as much as 14% have been reported by Featherston and Neighbours [Phys. Rev. **130**, 1324 (1963)] for a sample containing 0.1 wt.% of oxygen.

TABLE II. Comparison of fit to "normal" and "anomalous" phonons.

Branch	Model	Total number of phonons[a] in rectangle[b] Anomalous	Normal	Number of negative misfits Anomalous	Normal	Average misfit in standard deviations Anomalous	Normal	Magnitude (per phonon) of misfit in normal group Std. Dev.	%	Average misfit in % Anomalous	Normal
Low	1	28	45	28	20	−2.5	+0.0	0.9	1.1	−3.4	+0.1
Low	2	28	45	26	10	−1.6	+0.9	1.2	1.4	−2.2	+1.0
High	1	15	30	15	13	−2.7	−0.1	0.7	0.8	−2.2	−0.1
High	2	15	30	13	7	−1.1	+0.7	1.2	1.2	−1.0	+0.8

[a] The rectangles containing these phonons are bounded by the following lines:

Low branch: $q_z=0.4$ and 0.9; $q_x=q_y=0.0$ and 0.3.
High branch: $q_z=0.1$ and 0.5; $q_x=q_y=0.15$ and 0.4.

[b] The high-branch rectangle included the corner of a second anomalous region; phonons in this region were not included.

tained on fitting the seven-neighbor model to *all* the phonons. More precisely, the values for these two cases differ by one error or less for ten of the force constants, between one and two errors for seven of the force constants, and between two and three errors for two constants (fifth neighbor α_1 and seventh neighbor β_1). Thus, the exclusion of the phonons in the anomalous regions has not materially affected this approximate, partial description of the forces.

(2) The forces are not axially symmetric.[17] None of the relations among the force constants of a given neighbor[18] imposed by axial symmetry are satisfied by these values to within the combined errors, the discrepancies being particularly marked for both fourth and seventh neighbors.

(3) The size of the forces varies in a sort of damped oscillatory manner as a function of interatomic distance. The second-neighbor force is quite large, actually slightly larger than that for first neighbors, and there is a marked sixth-neighbor force that is much larger than those for fourth, fifth, or seventh neighbors.

Anomalous Phonons

The anomalous regions, presented in terms of misfit to this model, are discussed at some length in the following section. It is important here to emphasize that the primary characteristics of these regions—their depth (or height) with respect to their immediate surroundings, their general shape, and their location in the plane—are real and not dependent on our particular exclusion of anomalous phonons from the least-squares evaluation of the model's force constants. This is illustrated in Table II, in which we compare the fit of two seven-neighbor models, (1) evaluated using only normal phonons, and (2) using all the phonons, to phonons in and around two major anomalous regions, the large low-branch depression away from symmetry axes and the high-branch depression crossing the [111] axis. The sample phonons were those in rather large rectangles centered on these depressions. It is seen that model 2 gives a markedly worse fit to the normal phonons than model 1, whereas neither model gives a satisfactory fit to the anomalous groups. The inclusion of the anomalous groups in the fitting of model 2 has averaged the misfits of the two groups of phonons in these areas, leading to lower calculated frequencies here than are given by model 1. Consequently, the normal phonons show a rimlike misfit to model 2, and the anomalous phonons show a less deep depression, but the depth of the depression measured from the rim is the same as for model 1. It then seems reasonable to describe the anomalous regions from a model that gives the best fit to the phonons that can be fitted, including those in these "rimlike" areas, which is what we have done.

DISCUSSION OF ANOMALOUS REGIONS

Summary of Observed Regions

The anomalous regions are outlined by the dashed curves in Figs. 3(c) and 3(d). The boundaries signify only that all the enclosed phonons have been excluded from the least-squares fit. The difference between experimental and calculated frequencies for each phonon is given in units of its standard deviation to show the significance of the misfit. The size of the misfit for the phonons in and near the anomalous regions is shown in the corresponding plots of Figs. 3(e) and 3(f), where each frequency difference is expressed as a percent of the calculated frequency. The boundaries here are estimates of contours of constant percentage misfit, as discussed below.

The combined observations of this study and the previous triple-axis studies identify eight anomalous regions which can be summarized as follows:

(1) The most prominent anomaly is the very strong depression of the phonon frequencies in both branches near the point (0,0,1). The extensive measurements of WC along the [111] and [100] axes show the depression to be steeply bounded in these directions, with a maximum depression of 11% of the calculated frequency (on the basis of the present seven-neighbor model).

[17] G. W. Lehman, T. Wolfram, and R. E. De Wames, Phys. Rev. 128, 1593 (1962).

[18] For third neighbors, $\beta_3=\alpha_1-\alpha_3$; for fourth neighbors, $\beta_1=\frac{1}{8}(\alpha_1-\alpha_2)=\frac{1}{8}\beta_2$; for seventh neighbors, $\beta_1=\frac{3}{8}(\alpha_1-\alpha_3)=\frac{1}{3}\beta_3$.

Woods[2] locates the anomaly along the [111] axis at $q_i \simeq 0.965$, but this apparently describes the point of maximum negative slope on the side of the depression since the minimum appears to be at or very near the limit $q_i=1$, i. e., (1,1,1), equivalent to (0,0,1). The present measurements include too few data in either branch to allow more than a crude guess as to the extent of the depression; the contours drawn in Figs. 3(e) and 3(f) are those guesses for contours of 2 and 4% misfit.

(2) There is a large depression in the low-branch frequencies centered approximately at (0.15,0.15,0.60). It does not fall on a symmetry axis, so it was not seen by WC. The present measurements give fairly good coverage of most of this area and show an oblong depression, at its deepest amounting to approximately 5%. The contours drawn are for 2 and 4% misfit.

(3) There is a narrow, troughlike depression in the high branch extending almost perpendicularly across the [111] axis, the center of the trough intercepting this axis at $q_i \simeq 0.29$. Woods[2] studied the corresponding dip in the [111] longitudinal dispersion curve and locates the anomaly at $q_i=0.27$, but this again appears to refer to the point of maximum slope, since the actual minimum appears to be consistent with the present results. The maximum depression is 3%.

(4) There is an enhancement of frequencies in the high branch in a region centered at $(\frac{1}{2},\frac{1}{2},0)$, the maximum difference being approximately 3%. The WC $[110]L$ data show similar behavior.

(5) There is a depression in the low branch near $(\frac{1}{2},\frac{1}{2},\frac{1}{2})$, the maximum difference observed being approximately 4%. Only a few data were obtained here, so the shape or extent of the region is very poorly known. An estimate of part of a 2% contour has been given. The few high-branch data here do not show such a depression, but the low-branch depression appears to include the point $(\frac{1}{2},\frac{1}{2},\frac{1}{2})$ at which the branches are degenerate, so the corresponding high-branch depression must be restricted to a smaller region around this point. The detailed $[111]L$ measurements shown by Woods support this general description and indicate that the maximum low-branch depression on this axis occurs at $q_i \simeq 0.53$.

(6) There is a broad ridge of frequency enhancement in the high branch extending almost perpendicularly across the [111] axis, the center of the ridge intercepting this axis at $q_i \simeq 0.40$. The frequency enhancement is small, the maximum difference being approximately 2%. The contour drawn here is for 1% misfit.

(7) The low branch shows a depression in a small region centered at $(\frac{1}{2},\frac{1}{2},0)$ that is flanked by regions of frequency enhancement. There is considerable uncertainty in this description, since experimental coverage of the area is quite incomplete; the present experimental technique could not reach any closer to the [110] axis for this branch than the data points shown, and the triple-axis measurements were made only along the axis. The present measurements show a region of frequency enhancement off the axis, the maximum difference being approximately 4%. The WC $[110]T_2$ data show frequency enhancement near $q_i=0.4$, the maximum being approximately 3%, followed by a depression that reaches approximately 5% at $(\frac{1}{2},\frac{1}{2},0)$. We have sketched a 2% contour around the depression and have drawn parts of a 2% contour for the regions of enhancement.

(8) Finally, by symmetry a low-branch phonon on the boundary at $(\frac{1}{2},\frac{1}{2},1-q_z)$ will have the same frequency as one at $(\frac{1}{2},\frac{1}{2},q_z)$ for $q_z<\sim\frac{1}{4}$, the limit being defined by the point of accidental degeneracy. The low branch should then show a depression of approximately 5% at $(\frac{1}{2},\frac{1}{2},1)$ and a region of frequency enhancement of as much as 4% near $(\frac{1}{2},\frac{1}{2},0.82)$. The few data obtained near $(\frac{1}{2},\frac{1}{2},1)$ suggest that this region of depression is quite small; an estimate of a 2% contour has been drawn. No data were obtained in the area where enhancement should be expected.

Predicted Kohn Anomalies

It has been suggested by Woods and colleagues that these anomalies in molybdenum are examples of Kohn anomalies,[19] caused by strong electron-phonon interactions, that give some image of its Fermi surface. As this seems the only reasonable suggestion, it would be nice to check it in detail. However, the present state of the theory of Kohn anomalies allows us to do little more than compare the positions of the anomalies and, with less confidence, their extent and general shape; predictions of absolute strengths are not possible. Even to do this much for a metal like molybdenum requires a somewhat involved discussion because of the complicated shape of its Fermi surface. The general features of the Fermi surface of molybdenum have been shown by the calculations of Lomer,[20] Loucks,[21] and Matthiess[22]; all were based on the APW method and gave approximately the same results. The few experimental data from magnetoacoustic attenuation and de Haas–van Alphen studies have been summarized recently by Sparlin and Marcus.[23] Combining these experimental data with the calculations of Loucks we obtain the $(1\bar{1}0)$ section of the Fermi surface shown in Fig. 4. The experimental data have changed a few dimensions and introduced a small amount of splitting due to spin-orbit coupling, but the general picture is that of the calculation: one band[24] with a large octahedral hole surface at H and smaller hole surfaces at N; a second band giving an electron "jack" centered at Γ; and a third band giving electron "lenses" centered on [001] axes.

[19] W. Kohn, Phys. Rev. Letters **2**, 393 (1959).
[20] W. M. Lomer, Proc. Roy. Soc. (London) **80**, 489 (1962); **84**, 327 (1964).
[21] T. L. Loucks, Phys. Rev. **139**, A1181 (1965).
[22] L. F. Matthiess, Phys. Rev. **139**, A1893 (1965). This calculation actually applies to tungsten.
[23] D. M. Sparlin and J. A. Marcus, Phys. Rev. **144**, 484 (1966).
[24] The symbols here are the customary group-theory notation of band-structure calculations. H refers to the zone boundary point (0,0,1); N, to the point $(\frac{1}{2},\frac{1}{2},0)$; and Γ, to the origin.

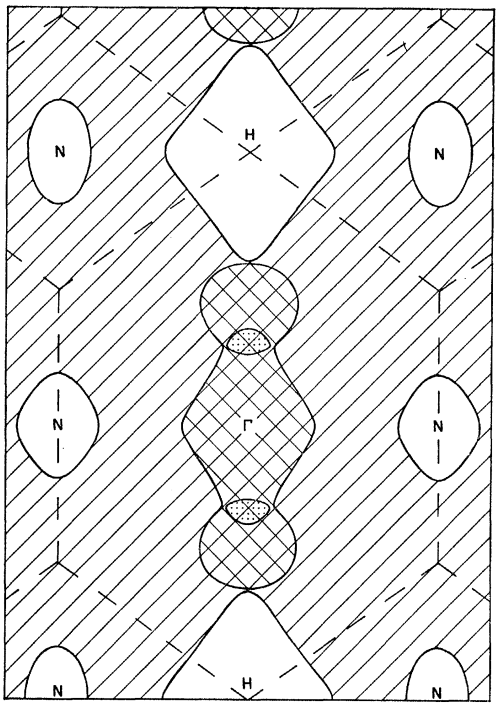

FIG. 4. A $(1\bar{1}0)$ section of the Fermi surface of molybdenum.

The geometrical construction of the loci of possible Kohn anomalies is straightforward in principle; an anomaly may occur for any wave vector $\mathbf{q}$ satisfying the relation

$$\mathbf{q}=\mathbf{k}_2-\mathbf{k}_1+\boldsymbol{\tau},$$

where $\mathbf{k}_2-\mathbf{k}_1$ extends between two points on the Fermi surface with parallel tangents, and $\boldsymbol{\tau}$ is a reciprocal-lattice vector. One thus locates all the points on the Fermi surface with a given tangent, plots all the possible wave vectors connecting these, and repeats this through the range of tangents. For a Fermi surface as complex as that of molybdenum the results in the $(1\bar{1}0)$ plane are a complicated set of overlapping curves. The difficult problem is to predict the shape and strength of the anomaly for the various parts of these curves. The available theoretical studies on anomalies associated with nearly spherical Fermi surfaces[25] and with surfaces of other geometries[26–28] have led us to the following six rules:

(1) The larger the radii of curvature at the points on the Fermi surface, the stronger the anomaly. The shape of the anomaly depends on the shape of the Fermi surface at these points, changing from an $x \ln x$ behavior for spherical surfaces to a square-root singularity for cylindrical surfaces to a strong logarithmic depression of frequencies for planar surfaces.[26,28]

(2) An anomaly occurs only when the electron velocities at the two points are antiparallel, not when they are parallel.[28,29]

(3) An anomaly does not depend on whether the spanned Fermi surface is a hole surface or an electron surface.[29]

(4) The strength of an anomaly varies with the magnitude of the cosine of the angle between $\mathbf{q}$ and the electron velocity at either point (which is normal to the Fermi surface), where $\mathbf{q}$ is a wave vector in a first Brillouin zone.[27]

(5) Polarization-dependent factors can produce strong variations in the strength of an anomaly along a given curve which may be quite different for the different branches.[25]

(6) If $\mathbf{k}_2-\mathbf{k}_1$ extends between a hole surface and an electron surface whose radii of curvature are nearly equal (i.e., so the surfaces can almost nest), the anomaly should appear as a strong depression of frequencies, similar to that associated with a pair of almost planar surfaces, even though the radii of curvature are not large.[28]

Using these rules we have estimated which parts of the curves tracing the loci of possible Kohn anomalies in the $(1\bar{1}0)$ plane of molybdenum should be or could be relatively strong. The results are shown as the 9 sections of curves drawn in Fig. 5. In the same figure are traced the various contour lines of Figs. 3(e) and 3(f), the low-branch contours being shown by long dashes and the high-branch contours by short dashes.

Curve 1 arises from vectors spanning the hole octahedron. The splitting arises from the inflection points in the $(1\bar{1}0)$ section of this surface. The sections of surface involved for the nearly linear majority of the curve are thought to be almost planar, so the anomaly here should be a rather strong depression of frequencies.

Curve 2 arises from vectors spanning the body of the electron jack. For vectors near the [111] axis the surfaces involved are thought to be almost planar, giving a strong depression of frequencies. For vectors near the [110] axis the surfaces appear to be almost cylindrical, so the anomaly should have changed here to a weaker, square-root–like behavior, with an enhancement of frequencies for wave vectors extending beyond this curve.

Curve 3 arises from vectors spanning end to end along the electron jack. The surfaces involved appear to be spherical, but with fairly large radii. The anomaly is probably the weakest of those included here, with an $x \ln x$ shape.

Curve 4 arises from vectors extending from an electron lens to the hole octahedron. The radii of curvature of the two surfaces appear to be nearly equal, giving a

[25] S. H. Vosko, R. Taylor, and G. H. Keech, Can. J. Phys. **43**, 1187 (1965), and the references contained therein.
[26] A. M. Afanas'ev and Yu. Kagan, Zh. Eksperim. i Teor. Fiz. **43**, 1456 (1962) [English transl.: Soviet Phys.—JETP **16**, 1030 (1963)].
[27] P. L. Taylor, Phys. Rev. **131**, 1995 (1963).
[28] L. M. Roth, H. J. Zeiger, and T. A. Kaplan, Phys. Rev. **149**, 519 (1966).
[29] Taylor's statements to the contrary (Ref. 27) have since been withdrawn [P. L. Taylor (private communication)].

depression of frequencies whose strength depends on how well the two surfaces nest. The anomaly is probably strongest near the start of the curve on the [001] axis and diminishes fairly quickly with distance along the curve, but we do not know how to estimate this extent with any accuracy; the length of the curve shown here is a guess based on angular factors and on the increasing mismatch of the surfaces for points farther away from the [001] axis.

Curve 5 arises from vectors extending between the almost flat parts of the electron jack and the hole octahedron. Both surfaces have fairly large sections that are thought to be almost planar whose orientations appear not too different, so there could be a strong depression of frequencies if parts of these almost planar sections are parallel, despite the relatively unfavorable angular factors. The extent of the curve shown is again only a guess based on angular factors and on an estimate of the limits of the almost planar parts of the electron jack.

Curve 6 arises from vectors extending from the hole octahedron to the hole surface at N. One of the surfaces is almost planar so the anomaly may not be negligible. We do not know the shape to be expected.

Curve 7 arises from vectors extending from the electron jack to the hole surface at N. The sections of the electron jack involved have surfaces ranging from almost flat to almost cylindrical, so the anomaly may not be negligible. We do not know the shape to be expected.

Curves 8 and 9 arise from vectors extending from sections of the knobs on the electron jack to the hole surface at N. In each case the radii of curvature appear to be nearly equal, so the associated anomaly could be a strong depression of frequencies.

Comparison of Observed and Predicted Anomalies

A comparison of the observed anomalies with these predicted Kohn anomalies show fairly good general correlation.

The large low-branch depression centered at (0.15,0.15,0.60) seems clearly to be the Kohn anomaly associated with curve 1; it is the type of anomaly expected here and follows reasonably well the general course of the curve, and it is the only anomaly in this area that is thought to be relatively strong. The limited extent of the depression along the curve must be the result of the polarization-dependent factors noted earlier. The good agreement between the curve and the observed region of greatest depression allows one to conclude that the dimension of the hole octahedron in this direction given in Fig. 3 must be reasonably accurate. In the [114] direction this diameter[14] is approximately 0.64.

The narrow, troughlike depression in the high branch extending across the [111] axis appears to be a combination of the anomalies for both curves 1 and 2; each is expected to be the type of anomaly found here, and each curve runs more or less parallel to the observed

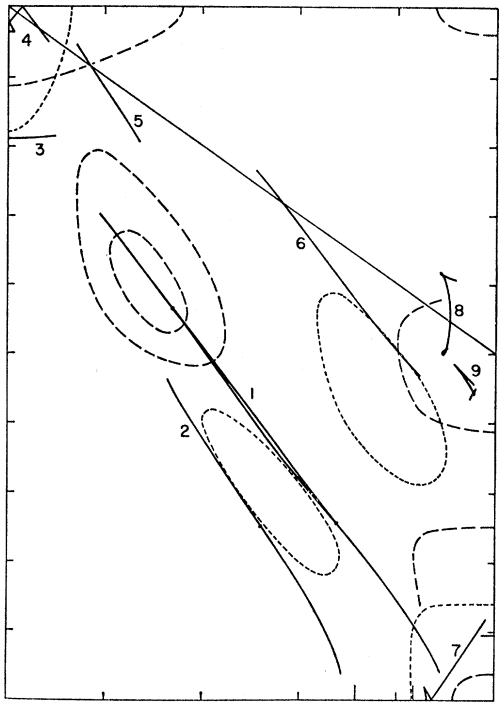

FIG. 5. A comparison of the predicted Kohn anomaly curves in the (1$\bar{1}$0) plane with the observed anomalous regions. The numbered solid curves showing the predictions are discussed in the text. The long-dash and short-dash curves are the misfit contours for the observed low-branch and high-branch anomalous regions, respectively.

depression. Woods[2] and Woods and Powell[3] interpreted the corresponding dip in the [111]L dispersion curve just as the anomaly for vectors spanning the hole octahedron, i.e., curve 1, but the surface of the electron jack in this direction is also thought to be almost planar, so the anomaly here for curve 2 does not appear to be negligible. Then, given the observed narrowness of the depression, we conclude that these two curves should be much closer together in this region, running more or less down the center of the depression, and thus that the dimensions of the electron jack and the hole octahedron in this direction should be approximately equal, roughly midway between the two different dimensions drawn in Fig. 3. In the [111] direction this diameter[14] would be approximately 0.50. This change will alter some of the other Kohn anomaly curves, notably curve 5, which will be shifted much closer to the point (0,0,1) and may show a stronger anomaly, and curve 7, which probably will move somewhat farther away from $(\frac{1}{2},\frac{1}{2},0)$.

The very strong depression near (0,0,1) was assumed by WC to be the anomaly for curve 5, but it could equally well be that for curve 4; each is expected to be the type of anomaly observed and to occur in this general area, and we do not know how to estimate directly their relative magnitudes or extent with any accuracy. No such depression has been observed in the

measured phonon dispersion of tungsten[30] or paramagnetic chromium,[31] which, when regarded in terms of the similarities and differences of their Fermi surfaces[21,22,32] to that of molybdenum, suggests that this depression for molybdenum is due primarily to the anomaly of curve 4. The argument is not conclusive, however; one can question, for example, whether the measurements on these elements were actually made in the appropriate areas or at close enough intervals to detect the anomalies, since one really does expect to observe some sort of curve 5 anomaly, at least for paramagnetic chromium, where the size and parallelism of the almost planar surfaces seems to be established as the key to the formation of its antiferromagnetic state. At present, one can say only that the depression could be due to either or both of these two anomalies.

We cannot offer a satisfactory detailed interpretation of the anomalous regions found in the two branches in the neighborhood of $(\frac{1}{2},\frac{1}{2},0)$. The two branches show different anomalies here, but there are three predicted Kohn anomaly curves in or near the area, so a correlation would seem possible. However, the very poor experimental coverage of the low-branch region and the various uncertainties as to shape, extent, position, and polarization dependence of the predicted anomalies introduce so many unknowns that our attempts to interpret these regions have amounted to little more than guesses. Triple-axis measurements of the phonon dispersion for tungsten show anomalous behavior in the low branch along the [110] axis that is quite similar to that shown by molybdenum. This suggests that the low-branch anomalous behavior in this region is not due primarily to the anomaly of curve 7, since one of the surfaces involved in this anomaly is the hole surface at N, which is believed to be much smaller in tungsten than in molybdenum.

The depression of frequencies in the low branch near $(\frac{1}{2},\frac{1}{2},\frac{1}{2})$ appears to be due to one or both of the anomalies of curves 8 and 9; each is expected to be the type observed here. The experimental coverage of this region is too limited to attempt any further interpretation.

Finally, the weak, broad ridge of frequency enhancement extending across the [111] axis in the high branch shows a limited correlation in extent and direction with curve 6 and thus may be due to that anomaly, perhaps in combination with the nearby anomalies of curves 8 and 9. The type of anomaly to be expected for curve 6 was not known.

SUMMARY AND CONCLUSIONS

The present study of molybdenum has yielded frequency–wave-vector values for 354 phonons, in two branches, distributed irregularly in the rectangular elemental area of the $(1\bar{1}0)$ plane, with an average effective error in frequency of 1.6%. These data are in reasonably good agreement with the symmetry-axis measurements of WC. Attempts were made to determine the interatomic restoring forces by fitting Born–von Karman general force models to these data, but the phonons in several regions in each branch showed anomalous behavior, demonstrating that the effective forces include significant components whose range is too long to allow analysis from these data. We have instead obtained a partial description of the forces by restricting the least-squares fitting procedure to those phonons that could be fitted, ignoring the data in the anomalous regions, and have then tried to interpret separately the anomalous regions.

Our results for the partial description of the restoring forces differ from those of WC. These investigators, who excluded the phonons in the region of the strong anomaly near (0,0,1) from their analysis, reported a reasonably good fit for an axially symmetric, third-neighbor model, and the fit was not very much improved when more distant neighbors were included; whereas in our study, after excluding the phonons in eight anomalous regions, an acceptable fit was obtained only for models including at least six neighbors. This difference is at least partly due to the difference in the coverage of the Brillouin zone in the two experiments. For example, the relatively large sixth-neighbor force constant causes particularly noticeable effects in the high branch in a rather large region in the $(1\bar{1}0)$ plane that extends across the [111] axis between $q_i \simeq 0.65$ and 0.85, the frequencies in this region being higher than those calculated from a fitted third-neighbor model. The WC data include only two phonons in this region, and the positive discrepancy both show may not seem important, but the present measurements include approximately 20 phonons in this region that all show positive misfit to the third-neighbor model, making it quite clear that longer-range forces must be included to describe adequately these "normal" phonons. The model of the present study gives a better fit to phonons in a much larger fraction of the plane and allows a clear picture of the anomalous regions arising from still longer range forces, so it is thought to be preferable. The force-constant values found for this model do not show axial symmetry. They vary radially in a more or less damped oscillatory manner, with a quite large sixth-neighbor value, which is probably a result of the same electron-phonon interactions that are thought to be the origin of the longer-range forces of the anomalous regions.

The anomalous regions are an interesting and important feature of the phonon dispersion in molybdenum, both because of the effects displayed and because of the appreciable fraction of phonons affected. They appear to be examples of Kohn anomalies, as suggested by WC, in that we are able to propose cor-

[30] S. H. Chen and B. N. Brockhouse, Solid State Commun. 2, 73 (1964).

[31] H. B. Møller and A. R. Mackintosh, in *Proceedings of the Bombay Symposium on Inelastic Scattering of Neutrons* (International Atomic Energy Agency, Vienna, 1965), Vol. 1, p. 95. The sample temperature for the data presented is not stated.

[32] T. L. Loucks, Phys. Rev. 143, 506 (1966).

relations with predicted Kohn anomalies that in most cases seem quite plausible. We find, however, that in many of these regions more than one Kohn anomaly could or should be contributing strongly, and we have no reliable way of predicting their relative strengths. Ignorance of the shape or extent of some of the predicted Kohn anomalies and poor experimental coverage of several of the anomalous regions add to the difficulty of a detailed interpretation. There are only two regions —the low-branch large depression away from symmetry axes, and the high-branch troughlike depression crossing the [111] axis—where the interpretation seems clear enough to allow us to draw Fermi-surface dimensions from the observations. The little or no overlap of these two regions shows the importance of the polarization-dependent factors. In both these regions the Kohn anomalies arise from vectors between almost planar surfaces, so the Kohn anomalies are actual depressions of frequency, not singularities in slope, and the appropriate Fermi-surface diameters are measured to the bottoms of the depressions. The results support the Fermi-surface calculations of Loucks but suggest that in the [111] direction the diameters of the hole octahedron and the body of the electron jack should be more nearly equal. The prominent strong depression near (0,0,1) has two possible origins of unknown relative strengths.

Several of these anomalies should also occur in tungsten and paramagnetic chromium, since their Fermi surfaces are very similar to that of molybdenum. Each, for example, should have a low-branch depression away from symmetry axes and a high-branch depression crossing the [111] axis. In tungsten, one can predict fairly accurately the course of its Kohn anomaly curves 1 and 2, since the appropriate Fermi-surface dimensions are known experimentally,[33] so measurements of these two anomalous regions could be given a quantitative check of their interpretation and, for the high-branch region, might give some information on the relative contributions of the two anomalies since they are separated appreciably here. In chromium, one may be able to alter considerably both these anomalous regions simply by lowering the temperature below the Néel temperature 38.5°C, since the onset of its antiferromagnetic state is believed to modify drastically the large planar sections of its Fermi surface,[34] so measurements here could yield a rather interesting verification of the origin of these regions in addition to giving the first experimental values for these paramagnetic Fermi-surface dimensions. The magnitudes of the anomalies in these elements should be expected to be small, of the order of a few percent, so it is not surprising that the triple-axis measurements of phonon dispersion made at fairly large intervals along symmetry axes have revealed only one anomaly (that in the low branch at $[\frac{1}{2},\frac{1}{2},0]$) in tungsten and none in chromium; they are small enough that one must generally be looking for them to observe them.

ACKNOWLEDGMENTS

C. B. W. wishes to express his thanks to the John Simon Guggenheim Foundation for the Fellowship that made possible the stay at Harwell during which this investigation was undertaken, and his appreciation to Dr. E. Bretscher, head of the Nuclear Physics Division, for the hospitality and support offered him. We are grateful to Dr. G. L. Squires for several discussions, to Dr. D. Long Price and Dr. S. Sinha for their help and advice with the experiment, and to the members of the Pile Neutron Research group at Harwell for their assistance and cooperation.

APPENDIX: EXPERIMENTAL CORRECTIONS

The program for calculating the major correction does the following: For a given mean direction and magnitude of the incident wave vector relative to the crystal and for a given mean scattering angle to the detector, the observed mean magnitude of the scattered wave vector of a given phonon group k_{obs}' is corrected to yield the scattered wave-vector magnitude that would have been observed with single-ray geometry (i.e., zero angular divergence and wavelength spread) and zero mosaic spread. The additive correction is

$$\Delta k' = k_c' - \frac{\int\int\int\int\int F(\theta,\phi,\theta',\phi',\Delta k_0)\, k'(\theta,\phi,\theta',\phi',\Delta k_0) \sin\theta \sin\theta' d\theta d\theta' d\phi d\phi' d\Delta k_0}{\int\int\int\int\int F(\theta,\phi,\theta',\phi',\Delta k_0) \sin\theta \sin\theta' d\theta d\theta' d\phi d\phi' d\Delta k_0},$$

where θ, ϕ and θ', ϕ' are the usual polar angular variables describing the deviations of the directions of incident and scattered rays, respectively, from their central ray directions, and Δk_0 describes the variation in magnitude of the incident wave vector from its mean value. The quantity $k'(\theta,\phi,\theta',\phi',\Delta k_0)$ is the magnitude of the scattered wave vector, a function of the five variables, that is determined by the conservation equations,

$$(\hbar^2/2m)(k'^2 - k_0^2) = \hbar\omega(\mathbf{q}),$$
$$\mathbf{k}' - \mathbf{k}_0 = \boldsymbol{\tau} + \mathbf{q},$$

where $\omega(\mathbf{q})$ is obtained by solving the secular equation using preliminary values for the force constants in a

[33] W. M. Walsh and C. C. Grimes, Phys. Rev. Letters **13**, 523 (1964).

[34] See, for example, L. M. Falicov and M. J. Zuckerman, Phys. Rev. **160**, 372 (1967).

seven-neighbor Born–von Karman general force model; k_c' is just the central ray solution $k'(0,0,0,0,0)$. The weighting factor F is

$$F=\exp\left(-\tfrac{1}{2}\left[\left(\frac{\theta}{\sigma_1}\right)^2+\left(\frac{\theta'}{\sigma_2}\right)^2+\left(\frac{\Delta k_0}{\sigma_3}\right)^2\right]\right)$$
$$\times\frac{\{(\mathbf{k}'-\mathbf{k}_0)\cdot\mathbf{e}(\mathbf{q})\}^2}{\omega^2}\frac{k'}{k_0}\frac{[1-\exp(-4.07k_0/k')]}{|J|},$$

where σ_1, σ_2, and σ_3 are experimental parameters describing the combined incident-beam angular divergence and sample mosaic spread, the scattered-beam angular divergence, and the incident wavelength spread in terms of assumed Gaussian shapes, respectively; the bracketed term gives an approximate representation of the wavelength dependence of the detector sensitivity; and the remaining terms arise from factors in the one-phonon differential scattering cross section. (We have ignored any variation of the Debye-Waller factor, which should be small here, and we have assumed equipartition of energy, which should be valid for the small wave-vector phonons for which the correction is important.)

For our experiment, $\sigma_1=0.01228$ rad, $\sigma_2=0.00818$ rad, and $\sigma_3/k_0=0.0329$. The correction appears to be important only for the shorter wave-vector phonons, the largest correction causing the ratio ν/q to be reduced approximately 5%. The correction almost always caused a reduction in the ratio ν/q. Where the second transverse branch is nearly degenerate with the low branch in the small q region, the correction had to be calculated for both branches and combined to yield the appropriate correction to the observed k'. Most of the numerical integrations were done for 3888 points in the five-dimensional space; rechecks of a number using a finer mesh involving 19 800 points showed the coarser calculation to be good to 10%.

PHYSICAL REVIEW VOLUME 177, NUMBER 3 15 JANUARY 1969

Magnetoacoustic Effect in Mercury†

TOMMY E. BOGLE,* JULIAN B. COON,‡ AND CLAUDE G. GRENIER
Department of Physics, Louisiana State University, Baton Rouge, Louisiana 70803
(Received 27 May 1968)

Geometric resonances in the ultrasonic attenuations have been observed in high-purity mercury single crystals with longitudinal sound waves propagated along five crystallographic directions at frequencies up to 165 MHz. Of the five, only data for the $(1\bar{1}0)$, (110), and $(11\bar{2})$ directions are reported. The dominant resonance branches have been assigned to calipers of the second-band electron-lens surface, with three major symmetry calipers being obtained. The remainder of the resonance branches have been assigned to orbits on the first-band hole surface. Various breakthrough dimensions of the hole surface were determined from these orbits. The pseudopotential coefficients corresponding to the planes bounding the first Brillouin zone in mercury have been estimated by comparing the geometric resonance data with the results of a four-pseudowave calculation neglecting spin-orbit coupling.

I. INTRODUCTION

THE Fermi surface of crystalline mercury has been studied both experimentally and theoretically by a number of investigators in the past few years. The de Haas–van Alphen (dHvA) effect has yielded several extremal cross sectional areas[1]; extremal calipers of a portion of the surface have been determined from preliminary magnetoacoustic data[2]; effective masses on the Fermi surface have been determined from an Azbel-Kaner cyclotron resonance experiment[3]; and information about the topology has been obtained from magnetoresistance measurements.[4,5] The first theoretical determination of the band structure was a three plane wave pseudopotential calculation[1] based on the dHvA data. An empirical four parameter model[5] based on magnetoresistance data was later presented and used as a starting point, along with the dHvA data, for an eight plane wave pseudopotential calculation including spin orbit coupling and constrained to satisfy the requirement of compensation.[5] A detailed relativistic

† The financial assistance received from the Dr. Charles E. Coates Memorial Fund of the Louisiana State University foundation donated by George H. Coates for the preparation of this manuscript is gratefully acknowledged. Report No. ORO-3087-30 is prepared under U. S. Atomic Energy Commission Contract No. AT-(40-1)-3087. Part of this work was submitted by one of us (T.E.B.) as partial fulfillment of the requirements for the Ph.D degree in physics at Louisiana State University.

* Present address: Department of Physics, McNeese State College, Lake Charles, La.

‡ Present address: Department of Physics, University of Houston, Houston, Texas.

[1] G. B. Brandt and J. A. Rayne, Phys. Rev. **148**, 644 (1966).

[2] T. E. Bogle, C. G. Grenier, and J. M. Reynolds, Bull. Am. Phys. Soc. **2**, 183 (1967).

[3] A. E. Dixon and W. R. Datars, Solid State Commun. **3**, 377 (1965).

[4] W. R. Datars and A. E. Dixon, Phys. Rev. **154**, 576 (1967).

[5] J. M. Dishman and J. A. Rayne, Phys. Rev. **166**, 728 (1968).